THE ISO LWS BEAM PROFILE

C. Lloyd

Rutherford Appleton Laboratory, Chilton, Didcot, Oxon OX11 0QX, UK

ABSTRACT

The methods used to derive the LWS beam profile are described and the effective apertures of the LWS detectors are given. The extended source correction factors and conversions from flux to MJy sr^{-1} are also given. The apertures are found to be smaller than expected.

Key words: ISO: LWS – LWS: beam profile – LWS: extended source correction

1. INTRODUCTION

The mean beam profile, and with it the effective solid angle, of the detectors is required as part of the calibration of extended source fluxes. The effective solid angle is also required in the determination of the point/extended source flux correction. Both of these are necessary for the conversion of observed flux to MJy sr^{-1} for extended sources and for the calibration of sources observed in parallel and serendipity mode.

The mean beam profile is derived from a series of standard bias, grating scan observations of Mars. One observation was made on axis and the others were distributed around the field as shown in Figure 1. The mean flux in each detector at each of the offset positions is used to describe the radial sensitivity of the instrument and a parameterisation defines the mean beam profile. In addition subsets of the data along the four radial alignments, which are labelled PA30, PA75, PA120 and PA165 on Figure 1, have been analysed to investigate possible asymmetries in the beam profile.

The data used to determine the mean beam profile are from a special processing with OLP v8. The data are flux calibrated in the standard way and then de-fringed. The profiles are determined for each detector and are normalised to the flux observed on axis.

1.1. Optics

The optical train of the LWS consist of the contour field mirror (CFM) that allows a beam of $\sim 120''$ to fall on the complex mirror M2 which is inclined at ~ 22 degrees to the incoming beam. M2 then presents an elliptical beam of $\sim 105 \times 97''$ (nominal FWHM) to the collimator, the LWS entrance pupil, the re-imaging mirror and detectors. Immediately in front of each detector is a rectangular aperture with rounded ends which, when projected onto the sky, are approximately elliptical with dimensions of $104 \times 157''$ at SW1 and $138 \times 131''$ at LW5 in the 'along' and 'across' dispersion directions respectively. The long and short axes of M2, projected onto the sky, are PA30 and PA120 (Y and Z axes) respectively.

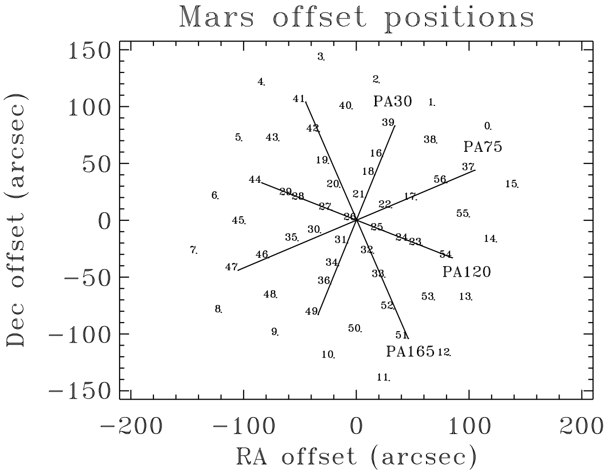

Figure 1. Offset positions of the Mars beam profile observations.

As the detector apertures are nominally larger than the incoming beam from M2 it is, in fact, M2 that defines the aperture of the detectors, and the character of the optics determines the instrumental profile. The size of the aperture was initially assumed to be $100''$ (the size of M2) but it has become clear that the beam is significantly smaller than this, for reasons that are not known. Perversely, the substrate that supports M2 is also reflective, particularly at longer wavelengths, and is believed to be responsible for the fringing that is seen off axis. However, a second consequence of this is that the supposed aperture will have weak wings out to $\sim 120''$ diameter (the size of the CFM).

1.2. Known problems

The mean fluxes which are used to describe the mean beam profile conceal a wide range of variation with wavelength, principally due to spectrum fracturing and fringing. These are discussed in more detail in the accompanying paper (Lloyd 2003). In general the agreement between adjacent detectors (stitching) is good, and for the positions closest to the axis the relative flux is fairly constant. With increasing radius the relative flux becomes less constant and the fringing becomes more visible.

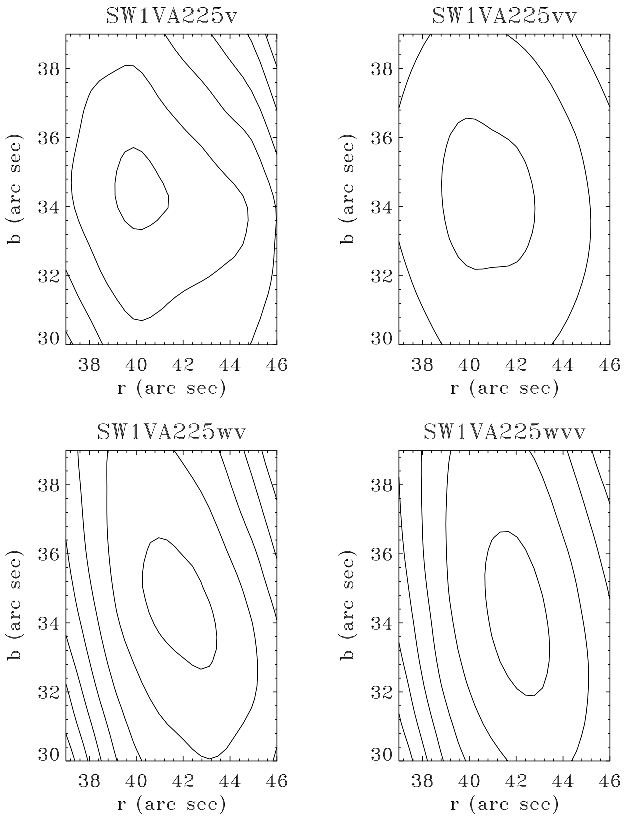

Figure 2. Contours of the goodness-of-fit measures for SW1. The top pair is in linear flux space and the lower pair in ln flux space. The left hand pair are the sums of absolute residuals and the right hand pair are the sums of the residuals squared. The contour levels are relative to the minimum and are the same in each plot.

However, in one sector the spectra take on a fractured appearance.

Beam size: From the earliest estimates of the beam size it has been recognised that the beam is narrower than expected. The reason for this is unknown.

Fringing: Fringing is seen in observations of extended sources and point sources observed off axis. Its effects increase with distance off axis, and with wavelength. Interference between the beam from M2 and its substrate are responsible.

Spectrum fracturing: Observations in one sector of the field, with negative RA and Dec offset (Figure 1), show a break down in the usually good stitching between adjacent detectors. The reasons are unknown.

Asymmetry: The mean beam profile is asymmetric, mainly due to the effects of spectrum fracturing, but there are smaller effects that naturally introduce an asymmetry. These are the mirror M2 which is seen at an angle, and the tripod support of the secondary mirror which causes a small asymmetry in the telescope PSF.

Non linearity: For some of the detectors, particularly LW3 Mars is a relatively strong source and the observations on, and close to, the axis suffer from saturation problems. At present these are not corrected.

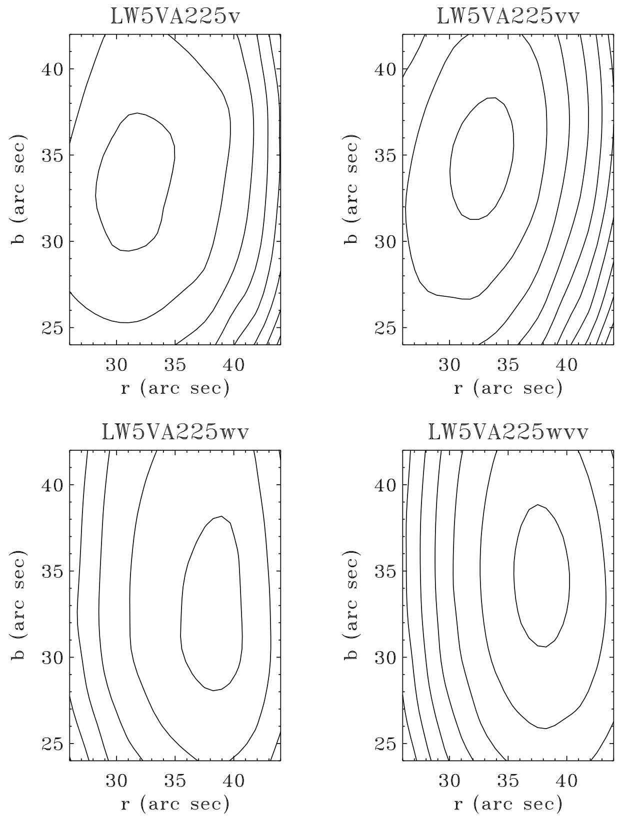

Figure 3. Contours of the goodness-of-fit measures for LW5.

Transients: None of the observations have been corrected for the transient response of the detectors, and this is general for the LWS.

2. THE MEAN BEAM PROFILE

To determine the effective beam size the de-fringed observed mean fluxes have been compared with fluxes derived from a convolution of the telescope PSF with apertures of various sizes. The apertures were assumed to have top-hat profiles. The latest models of the telescope PSF includes the effects of the central obscuration and its supporting structure, and indicate that the power in the Airy rings is increased and that the wings of the profile contain 2-D structure. The asymmetry introduced into the profile is due to the three-legged secondary support.

Early in this exercise it became clear that the nominal value of the aperture of $100''$ was too large. The best value for most of the detectors lies close to $80''$, and for LW3, LW4 and LW5 is somewhat smaller than this. At the longest wavelengths the width of the telescope PSF is larger than the aperture itself which makes these determinations more difficult. An uncertainty of one arc second in the radius corresponds to about 5% in the effective area of the aperture.

It also became clear that a simple circular aperture could not adequately describe the asymmetry in the beam which is described in more detail in the accompanying paper. These effects are due to some complex (and unknown) behaviour of the beam and not due to a relatively simple non-circular aperture. However, in order to model the beam in a simple way it has been necessary to introduce a non-circular aperture. Of the infinite choice available a composite semi-circular and semi-elliptical aperture has been used.

3. RESULTS

The convolution was performed over a range of radii r and semi-major/minor axes b of the components of the aperture. The aperture was always continuous so that one axis of the semi-elliptical part was always equal to the radius of the semi-circular part. Numerous experiments were performed to determine the best orientation of the aperture. The results were not particularly sensitive to the value chosen so ultimately this was fixed for all detectors.

For each convolution the observed, de-fringed fluxes were compared on a point by point basis with the calculated flux at each position in its correct location in the Y-Z plane of the telescope PSF, and the residuals calculated. To estimate the goodness-of-fit four different measures were used. These were (i) the sum of the absolute residuals, (ii) the sum of the squares of the residuals, both in linear flux, and (iii) and (iv) the same quantities in ln flux. There are several reasons for considering different measures. Firstly, the errors in fitting the observed fluxes are not Gaussian but dominated by systematic effects, such as the asymmetry in the beam, and under these circumstances the sum of the absolute residuals might give a less biased result. Also the weaker fluxes at the edge of the field are given disproportionately low weight in linear flux space. Ideally all four measures should point to the same set of aperture parameters but if they do not then they will give some indication of where the inconsistency lies.

The plots of the goodness-of-fit measures on the $r - b$ grids are given for SW1 and LW5 in Figures 2 and 3. In general there is some variation between detectors but for SW1 to LW2 there is reasonable agreement between the different measures of the goodness-of-fit. For LW3 to LW5, and SW5 there is a more systematic difference between the linear and ln flux measures, which indicates a systematic difference in the best-fit profile between the inner and outer part of the beam. There is also a considerable variation in the quality of the fit, both across the detectors and for the different measures of the goodness-of-fit. Under these circumstances any values of the best-fit parameters are a compromise, so the adopted values of r and b were taken to be where the volume of the figure described by the residuals passes through zero, in the region of the minima in the goodness-of-fit measures. Along this line various combinations of r and b are possible but over a sensible range the numerical uncertainty in the area of the aperture is $\sim 2\%$.

The relative mean flux at each of the observed offset positions (see Figure 1) is shown for each detector in Figure 4 with the convolution of the telescope PSF and the best fit composite aperture superimposed. At shorter wavelengths the telescope PSF is narrow enough to probe the structure of the rectangular (top-hat) instrumental profile and some indication its shape can be seen. As the telescope PSF broadens towards longer wavelengths the details of the instrumental profile become washed out and the observed profile becomes more Gaussian.

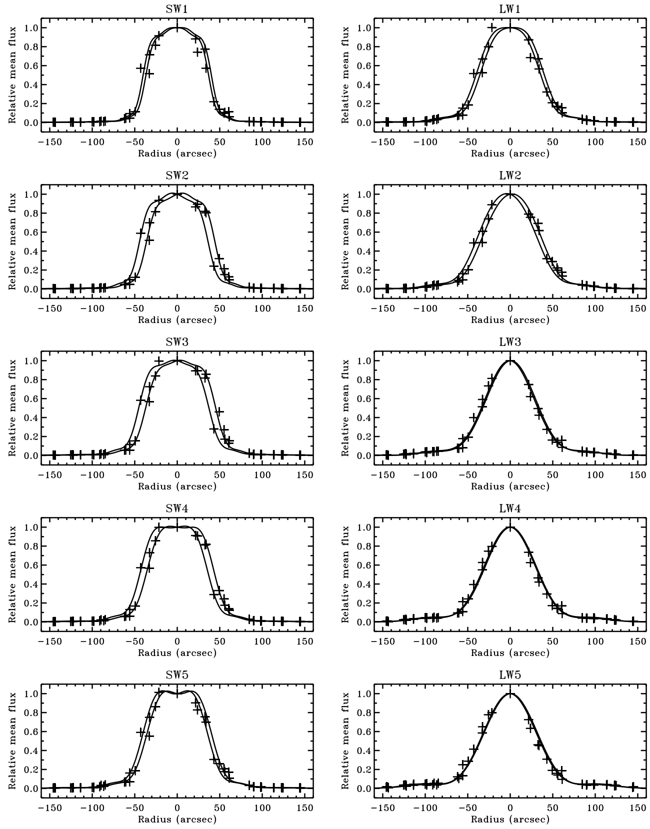

Figure 4. The mean beam profiles for each detector. The observed relative mean flux at each offset position is plotted against radius, with the sign taken from the RA offset in Figure 1. The lines on each plot show the calculated profile in the spacecraft Y and Z co-ordinates.

Table 1. Effective Aperture Radius.

Detector	Radius ($''$)	Detector	Radius ($''$)
SW1	39	LW1	38
SW2	42	LW2	39
SW3	43	LW3	35
SW4	41	LW4	34
SW5	40	LW5	33

3.1. Flux correction for extended sources

The LWS flux scale is based on a point source calibration, although beyond the diffraction limit at about 110μm a substantial fraction of the flux from an on-axis point source if diffracted out of the aperture. In fact there are significant diffraction losses for all LWS detectors but provided the calibration is applied to point sources observed on axis these losses are irrelevant. However, for (ideal) extended sources similar diffraction losses do not occur, and so a correction has to be applied to correctly place the derived fluxes on the point source calibration scale. To do this requires the effective aperture of each detector and the PSF of the telescope.

The extended source correction is the measure of the fraction of flux in the telescope PSF that lies within the detector aperture. For this the best-fit apertures are used which have a top-hat instrumental profile by definition. The correction factors are given in Table 2.

4. EXTENDED SOURCE FLUX PER UNIT AREA

To convert the observed fluxes of extended sources to MJy sr^{-1} requires both the extended source correction factor and the effective aperture explicitly.

Table 2. Extended source corrections and effective beam sizes.

Detector	f	$\omega * 10^6$	Detector	f	$\omega * 10^6$
SW1	0.88	0.114	LW1	0.69	0.107
SW2	0.88	0.130	LW2	0.69	0.111
SW3	0.84	0.135	LW3	0.62	0.092
SW4	0.73	0.117	LW4	0.55	0.088
SW5	0.70	0.114	LW5	0.48	0.083

The corrected extended source flux for an observed flux F (Jy),

$$S = F.f/(\omega * 10^6) \text{ MJy sr}^{-1}$$

where f is the extended source correction and ω is effective solid angle of the beam (sr).

However, these corrections are derived under the assumption of a smooth and very extended flux distribution. In the real world, structure or embedded sources could produce significant discrepancies from the ideal situation, and with it differences in flux.

4.1. COMPARISON WITH IRAS

LWS observations have been made at a number of positions in the Trumpler 14 and 16 fields and these have been compared with the IRAS 100μm fluxes at the same positions. Both fields contain a large area of extended emission, which although relatively smooth, does change by a factor of 2 – 3 within each region. Figure 5 shows the comparison of the converted LWS and IRAS 100μm fluxes using the current LWS calibration and these measurements give a mean ratio, LWS/IRAS $\sim$ 0.9$\pm$0.2. Ideally for this comparison the extended flux should be distributed as evenly as possible, and part of the uncertainty is probably due to unresolved structure within the beam.

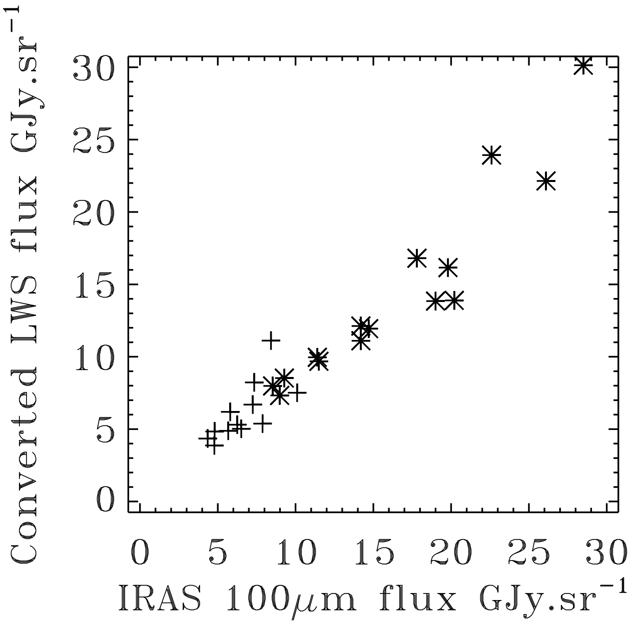

Figure 5. Comparison of converted LWS and IRAS 100 μm extended source fluxes in the Trumpler 14 (+) and 16 (*) fields.

For fields containing multiple sources the observed flux will depend critically on the positions of the sources relative to the optical axis. To recover or model the observed flux will require positional information on the sources and a deconvolution with the telescope PSF and instrumental profile. Indeed, for single point sources observed off axis a similar procedure will be required to recover the correct flux.

REFERENCES

Lloyd, C., 2003, this volume